The Deuteron Tensor Structure Function b_1

A Proposal to Jefferson Lab PAC-40
(Update to PR12-11-110)

K. Allada,   A. Camsonne,   J.-P. Chen,[†]
A. Deur,   D. Gaskell,   M. Jones, C. Keith, J. Pierce,
P. Solvignon,[†]   S. Wood,   J. Zhang
Thomas Jefferson National Accelerator Facility, Newport News, VA 23606

O. Rondon Aramayo,[†] D. Crabb,   D. B. Day,
C. Hanretty,   D. Keller,[†] R. Lindgren, S. Liuti, B. Norum,
Zhihong Ye,   X. Zheng
University of Virginia, Charlottesville, VA 22903

N. Kalantarians[†]
Hampton University, Hampton VA 23668

T. Badman, J. Calarco, J. Dawson,
S. Phillips,   E. Long,[†] K. Slifer[†‡],   R. Zielinski
University of New Hampshire, Durham, NH 03861

G. Ron
Hebrew University of Jerusalem, Jerusalem

W. Bertozzi,   S. Gilad,   J. Huang
A. Kelleher,   V. Sulkosky
Massachusetts Institute of Technology, Cambridge, MA 02139

[†]Spokesperson
[‡]Contact

J. Dunne, D. Dutta

Mississippi State University, Mississippi State, MS 39762

K. Adhikari

Old Dominion University, Norfolk, VA 23529

R. Gilman

Rutgers, The State University of New Jersey, Piscataway, NJ 08854

Seonho Choi,   Hoyoung Kang,   Hyekoo Kang,   Yoomin Oh

Seoul National University, Seoul 151-747 Korea

H. P. Cheng,   H. J. Lu,   X. H. Yan

Institute of Applied Physics, Huangshan University, Huangshan, P. R. China

Y. X. Ye,   P. J. Zhu

University of Science and Technology of China, Hefei 230026, P. R. China

B. T. Hu, Y. Zhang

Lanzhou University, Lanzhou, P. R. China.

Abdellah Ahmidouch

Department of Physics, North Carolina A & T State University, Greensboro, NC 27401

Caroline Riedl

DESY, Notkestrasse 85, 22603 Hamburg, Germany

Abstract

The leading twist tensor structure function b_1 of spin-1 hadrons provides a unique tool to study partonic effects, while also being sensitive to coherent nuclear properties in the simplest nuclear system. At low x, shadowing effects are expected to dominate b_1, while at larger values, b_1 provides a clean probe of exotic QCD effects, such as hidden color due to 6-quark configuration. Since the deuteron wave function is relatively well known, any novel effects are expected to be readily observable. All available models predict a small or vanishing value of b_1 at moderate x. However, the first pioneer measurement of b_1 at HERMES revealed a crossover to an anomalously large negative value in the region $0.2 < x < 0.5$, albeit with relatively large experimental uncertainty.

We will perform an inclusive measurement of the deuteron tensor asymmetry in the region $0.16 < x < 0.49$, for $0.8 < Q^2 < 5.0$ GeV^2. With 30 days of 11 GeV incident beam, we can determine b_1 with sufficient precision to discriminate between conventional nuclear models, and the more exotic behavior which is hinted at by the HERMES data. The UVa solid polarized ND$_3$ target will be used, along with the Hall C spectrometers, and an unpolarized 115 nA beam. An additional 10.8 days will be needed for overhead. This measurement will provide access to the tensor quark polarization, and allow a test of the Close-Kumano sum rule, which vanishes in the absence of tensor polarization in the quark sea. Until now, tensor structure has been largely unexplored, so the study of these quantities holds the potential of initiating a new field of spin physics at Jefferson Lab.

Foreword

This proposal is an update to PR12-11-110 which was submitted to PAC38. For convenience, we reproduce the PAC report on the next page. We provide here an overview of the actions we've taken to address the PAC concerns. Full details are available in the main text.

As suggested by PAC38, we have modified our experimental technique to measure the tensor asymmetry instead of the cross section difference. This takes the simplified form of the ratio of tensor polarized to unpolarized cross-sections shown in Eq. 19. While this cancels the largest first order effects*, special care will be needed to control the sensitivity of the integrated counts in each state to time dependent drifts in detector response, charge measurement and luminosity.

We have assumed a tensor polarization (P_{zz}=20%) which is larger than the previous proposal. This assumption is based on the documentation of tensor polarized targets previously discussed in publications, and is supported by the experience of the collaboration's polarized target groups. This will require incremental development of existing DNP techniques. We acknowledge that less established methods, such as the 'hole-burning' technique recommended by the PAC, hold very good potential to produce significantly higher tensor polarization, but this will require significant R&D. We have initiated this process, although from a practical perspective, the funding for this development will likely remain limited until an approved experiment demonstrates the need for these novel tensor polarized targets.

The x_B-coverage has been expanded, although we note that a significantly non-zero value of b_1 at any x_B would unambiguously confirm its non-conventional behavior. Finally, we have engaged several theorists for calculations and to confirm that our interpretation of the relationship between the measured asymmetry and the tensor structure function b_1 is valid.

---

*For example, the target magnetic field will be oriented along the beamline during both polarized and unpolarized data taking, which greatly reduces the sensitivity to changes in acceptance in the two configurations.

PAC38 Report

PR12-11-110 "The Deuteron Tensor Structure Function b1"

Motivation: This proposal, a follow-up of LOI-11-003 submitted to PAC37, is dedicated to the measurement of the deuteron tensor structure function b_1 by measuring deep inelastic scattering from a tensor polarized deuterium target. All available models predict a small or vanishing value of b_1 at low x, however the first pioneering measurement of b_1 at HERMES revealed a crossover to an anomalously large negative value, albeit with a relatively large experimental uncertainty. This justifies the intention to make a precise measurement: confirmation that b_1 is relatively large may then require an explanation based on more exotic models for the deuteron, such as hidden color due to a 6-quark configuration.

Measurement and Feasibility: The collaboration proposes to carry out this experiment in Hall C, using the polarized UVa/JLab ND_3 target, the HMS/SHMS spectrometers and an unpolarized 115 nA electron beam. The tensor structure function b_1 is derived from the measurement of the difference between the transversely and longitudinally tensor polarized cross-sections, which is directly proportional to b_1 itself. From the measured value of b_1 the tensor asymmetry A_{zz} can be calculated, provided the structure function F_1 is known. The collaboration proposes to perform the measurement in 28 days of data taking at 11 GeV at the two x values of 0.3 and 0.5, which cover the range in which the HERMES data display the crossover of b_1 to large negative values.

Issues: Despite the interesting physics case presented, the PAC has identified several issues with this proposal.

1. One obvious problem is the theoretical interpretation of the results of this kind of experiments. Following the recommendation of PAC37 the collaboration has partially addressed this question by expanding the discussion of the expected behavior of $b_1(x)$ in various theoretical models. However to draw significant conclusions from this measurement, also given the limited kinematical coverage (see below) chosen, would require further work.

2. The chosen x range, although overlapping with the region in which the HERMES results were obtained, does not seem sufficient to determine $b_1(x)$ in such a way as to unambiguously establish its conventional or exotic behavior. The PAC encourages the collaboration to explore the possibility to carry out the measurement using a large acceptance spectrometer covering a wider x range.

3. The PAC has concerns about the proposed experimental method using the cross section difference between the transversely and longitudinally tensor polarized target configurations. Given a 5-tesla field for this type of target, the effect on the acceptance due to the target field for these configurations can be quite different, and such systematic uncertainties due to the acceptance and other effects may well be larger than the effect that the proponents are trying to measure.

4. The proponents should pursue the tensor asymmetry measurement technique. Currently, the proposed target has a rather low tensor polarization ($\sim$10%). It is crucial and important to pursue more vigorously techniques such as the RF "hole burning technique to improve the tensor polarization of the target.

Contents

1 Background and Motivation

The deuteron is the simplest nuclear system, and in many ways it is as important to understanding bound states in QCD as the hydrogen atom was to understanding bound systems in QED. Unlike it's atomic analogue, our understanding of the deuteron remains unsatisfying both experimentally and theoretically. A deeper understanding of the deuteron's tensor structure will help to clarify how the gross properties of the nucleus arise from the underlying partons. This provides novel information about nuclear structure, quark angular momentum, and the polarization of the quark sea that is not accessible in spin-1/2 targets.

In particular, a measurement of the deuteron's tensor structure function b_1 is of considerable interest since it provides a clear measure of possible exotic effects in nuclei, i.e. the extent to which the nuclear ground state deviates from being a composite of nucleons only [1]. Such a measurement is further motivated by its connection with the spin-1 angular momentum sum rule [2].

Jefferson Lab is the ideal place to investigate tensor structure in a deuteron target at intermediate and large x. We describe such a measurement in this proposal.

1.1 Tensor Structure of the Deuteron

When a spin 1 system such as the deuteron is subjected to a magnetic field along the z-axis, the Zeeman interaction gives rise to three magnetic sublevels $I_z = +1, 0, -1$ with population fractions p_+, p_-, p_0, respectively. These populations are described by both a vector polarization,

$$
\begin{aligned}
P_z &= \langle I_z/I \rangle \\
&= (p_+ - p_0) + (p_0 - p_+) = p_+ - p_-
\end{aligned}
\tag{1}
$$

and a tensor polarization [3]:

$$
\begin{aligned}
P_{zz} &= \langle 3I_z^2 - I(I+1) \rangle / I^2 \\
&= (p_+ - p_0) - (p_0 - p_-) = 1 - 3p_0
\end{aligned}
\tag{2}
$$

which are subject to the overall normalization $p_+ + p_- + p_0 = 1$.

Fig. 1 graphically demonstrates the dependence of the two nucleon distribution on the spin projection. If the two nucleons are in a relative $m = 0$ state, the surface of constant density is toroidal, while if they are in the $m = \pm 1$ state, the surface has a dumbbell shape.

In the case of deuteron spins in thermal equilibrium with the solid lattice, and neglecting the small quadrupole interaction [3], the tensor polarization is related to the vector polarization via:

$$
P_{zz} = 2 - \sqrt{4 - 3P_z^2}
\tag{3}
$$

The maximum absolute value of $P_{zz} = -2$ occurs only for vanishing populations in the $m = \pm 1$ states. If, on the other hand, only the $m = 1$ or $m = -1$ state are occupied, the vector polarization reaches its maximum value of $+1$, and $P_{zz} = +1$.
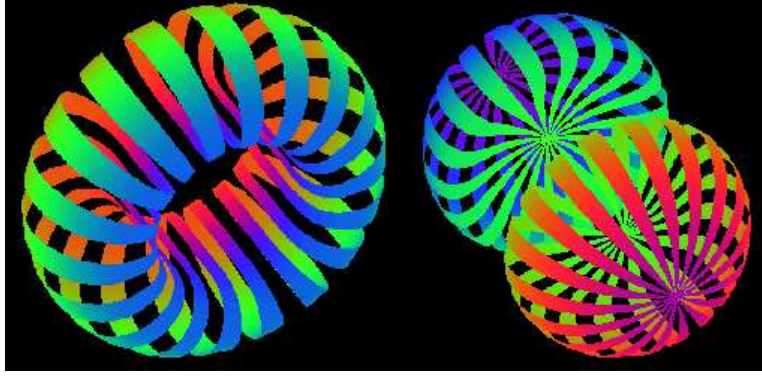
Figure 1: Nucleon densities of the deuteron in its two spin projections, $I_z = 0$ and $I_z = \pm 1$, respectively. *Reproduced from [4, 5].*

1.2 Deep Inelastic Scattering from Spin-1 Targets

Four independent helicity amplitudes are sufficient to describe virtual Compton scattering from a spin-1/2 target, after requiring parity and time reversal invariance. This number doubles for a spin-1 target, as the spin can be in three states (+, 0, -). This gives rise to a tensor structure which was first discussed for the deuteron for the real photon case by Pais [6], and later in the virtual photon case, by Frankfurt and Strikman [7]. Hoodbhoy, Jaffe and Manohar [8] introduced the notation which we now follow, whereby the tensor structure is described by the four functions b_1, b_2, b_3 and b_4. To summarize, the hadronic tensor can be decomposed as:

$$
\begin{aligned}
W_{\mu\nu} &= -F_1 g_{\mu\nu} + F_2 \frac{P_\mu P\nu}{\nu} \\
&\quad -b_1 r_{\mu\nu} + \frac{1}{6} b_2 (s_{\mu\nu} + t_{\mu\nu} + u_{\mu\nu}) \\
&\quad +\frac{1}{2} b_3 (s_{\mu\nu} - u_{\mu\nu}) + \frac{1}{2} b_4 (s_{\mu\nu} - t_{\mu\nu}) \\
&\quad +i\frac{g_1}{\nu} \epsilon_{\mu\nu\lambda\sigma} q^\lambda s^\sigma + i\frac{g_2}{\nu^2} \epsilon_{\mu\nu\lambda\sigma} q^\lambda (p \cdot q s^\sigma - s \cdot q p^\sigma)
\end{aligned}
\tag{4}
$$

where the purely kinematic expressions $r_{\mu\nu}$, $s_{\mu\nu}$, $t_{\mu\nu}$ and $u_{\mu\nu}$ can be found in [8]. The terms are all proportional to the polarization of the target E. The spin-1 structure functions F_1, F_2, g_1 and g_2 have the same expressions and are measured the same way as for a spin-1/2 target. The spin-dependent structure functions b_1, b_2, b_3, b_4 are symmetric under $\mu \leftrightarrow \nu$ and $E \leftrightarrow E^*$ and therefore can be isolated from F_1 and g_1 by unpolarized beam scattering from a polarized spin-1 target.

1.2.1 Interpretation in the Operator Product Expansion

In the Operator Product Expansion (OPE) framework, the leading operators $O_V^{\mu_1 \cdots \mu_n}$ and $O_A^{\mu_1 \cdots \mu_n}$ in the expansion are twist two. For a spin-1 target, the matrix elements of the time-ordered product

of two currents $T_{\mu\nu}$ have the following expressions:

$$
\begin{aligned}
< p, E|O_V^{\mu_1\cdots\mu_n}|p, E > &= S[a_n p^{\mu_1}...p^{\mu_n} + d_n(E^{*\mu_1}E^{\mu_2} - \frac{1}{3}p^{\mu_1}p^{\mu_2})p^{\mu_3}...p^{\mu_n}], \\
< p, E|O_A^{\mu_1\cdots\mu_n}|p, E > &= S[r_n \epsilon^{\lambda\sigma\tau\mu_1} E_\lambda^* E_\sigma p_\tau p^{\mu_2}...p^{\mu_n}]
\end{aligned}
\tag{5}
$$

The non-zero value of b_1 arises from the fact that, in a spin-1 target, the $\frac{1}{3}p^{\mu_1}p^{\mu_2}$ term doesn't cancel the tensor structure $E^{*\mu_1}E^{\mu_2}$. The coefficient d_n can be extracted from the comparison of $T_{\mu\nu}$ expansion and the spin-1 target hadronic tensor Eq. 4 as follows:

$$
\begin{aligned}
b_1(\omega) &= \sum_{n=2,4,...}^{\infty} 2C_n^{(1)} d_n \omega^n, \\
b_2(\omega) &= \sum_{n=2,4,...}^{\infty} 4C_n^{(2)} d_n \omega^{n-1},
\end{aligned}
\tag{6}
$$

for $1 \le |\omega| \le \infty$ (where $\omega = 1/x$). A Callan-Gross-type relation exists for the two leading order tensor structure functions:

$$
2xb_1 = b_2
\tag{7}
$$

valid at lowest order of QCD, where $C_n^{(1)} = C_n^{(2)}$. At higher orders, Eq. 7 is violated.

Sum rules can be extracted from the moments of the tensor structure functions:

$$
\begin{aligned}
\int_0^1 x^{n-1} b_1(x)\, dx &= \frac{1}{2} C_n^{(1)} d_n, \\
\int_0^1 x^{n-2} b_2(x)\, dx &= C_n^{(2)} d_n,
\end{aligned}
\tag{8}
$$

where n is even.

The OPE formalism is based on QCD and is target-independent. However, a target dependence is generated by Eq. 5, and spin-1 structure functions are subject to the same QCD corrections and their moments have the same anomalous dimensions as for a spin-1/2 target. In addition, the tensor structure functions should exhibit the same scaling behavior as F_1 and F_2, since they are generated from the same matrix element $O_V^{\mu_1\cdots\mu_n}$.

We focus in this document on the leading twist structure function b_1. A Callan-Gross type relation allows access to b_2 once b_1 is determined, and b_3 and b_4 do not contribute at leading twist.

1.2.2 Interpretation in the Parton Model

In the infinite momentum frame† of the parton model, the scattering of the virtual photon from a free quark with spin up (or down), which carries a momentum fraction x of the spin-m hadron, can be expressed through the hadronic tensor $W_{\mu\nu}^{(m)}$:

$$
W_{\mu\nu}^{(1)} = \left(-\frac{1}{2}g_{\mu\nu} + \frac{x}{\nu}P_\mu P\nu \right)\left(q_\uparrow^1(x) + q_\downarrow^1(x) \right) + \frac{i\epsilon_{\mu\nu\lambda\sigma}q^\lambda s^\sigma}{2\nu}\left(q_\uparrow^1(x) - q_\downarrow^1(x) \right),
$$

---

†All spins and momenta are along the z-axis.

9

for a target of spin projection equal to 1 along the z-direction, and:

$$W_{\mu\nu}^{(0)} = \left(-\frac{1}{2}g_{\mu\nu} + \frac{x}{\nu}P_\mu P\nu \right) 2q_\uparrow^0(x) \tag{9}$$

for a target of spin projection equal to zero along the z-direction. The tensor structure functions b_1 and b_2 can be expressed from the comparison of $W_{\mu\nu}^{(1)} - W_{\mu\nu}^{(0)}$ with Eq. 4 as follows:

$$b_1(x) = \frac{1}{2}\left(2q_\uparrow^0(x) - q_\uparrow^1(x) - q_\downarrow^1(x) \right) \tag{10}$$
$$b_2(x) = 2xb_1(x) \tag{11}$$

where $q_\uparrow^m$ ($q_\downarrow^m$) represents the probability to find a quark with momentum fraction x and spin up (down) in a hadron which is in helicity state m. The tensor structure function b_1 depends only on the spin-averaged parton distributions[‡]

$$q^1(x) = q_\uparrow^1(x) + q_\downarrow^1(x)$$
$$q^0(x) = q_\uparrow^0(x) + q_\downarrow^0(x) = 2q_\uparrow^0(x)$$

so it can be expressed as:

$$b_1(x) = \frac{q^0(x) - q^1(x)}{2} \tag{12}$$

Explicitly, b_1 measures the difference in partonic constituency in an $|m|=1$ target and an $m=0$ target. From this we see that while b_1 is defined in terms of quark distributions, it interestingly depends also on the spin state of the nucleus as a whole.

1.2.3   First Measurement of $b_1(x)$ by the HERMES Collaboration

The HERMES collaboration made the first measurement [9, 10] of b_1 in 2005. The experiment explored the low x region of $0.001 < x < 0.45$ for $0.5 < Q^2 < 5$ GeV^2. An atomic beam source was used to generate a deuterium gas target with high tensor polarization. The HERA storage ring provided 27.6 GeV positrons incident on the internal gas target.

As displayed in Fig. 2, the tensor asymmetry A$_{zz}$ was found to be non-zero at about the two sigma level, with an apparent zero crossing around $x = 0.3$. The tensor structure function b_1 exhibits a steep rise as $x \to 0$, which is qualitatively in agreement with the predictions of coherent double-scattering models. See for example Ref. [11]. The authors of Ref. [10] interpret the rapid rise at low x in terms of the same mechanism that leads to nuclear shadowing in unpolarized scattering, i.e. double scattering of the lepton, first from the proton, then from the neutron, with sensitivity to the spatial alignment of the two nucleons.

As is often the case with a pioneer measurement, the precision of the results leaves some room for ambiguity. Despite the surprisingly large magnitude and interesting trend of the data, all points

---

[‡]since, by parity, $q_\uparrow^m = q_\downarrow^m$
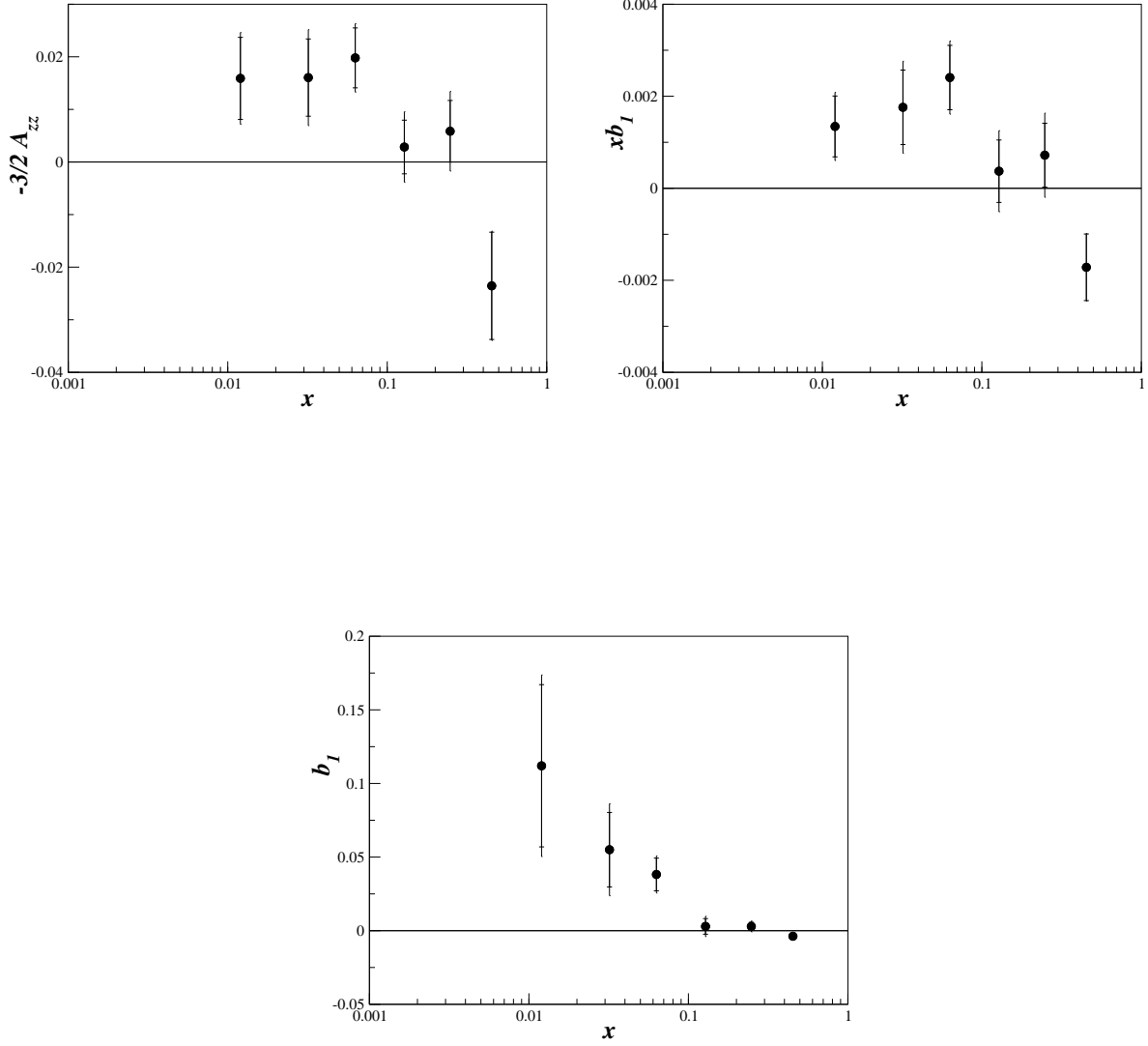
Figure 2: **Top**: HERMES [9] measurement of the inclusive tensor asymmetry $A_{zz}(x)$ and $xb_1(x)$ of the deuteron. **Bottom** : The tensor structure function $b_1(x)$ without x-weighting, which reveals a steep rise as $x \to 0$.
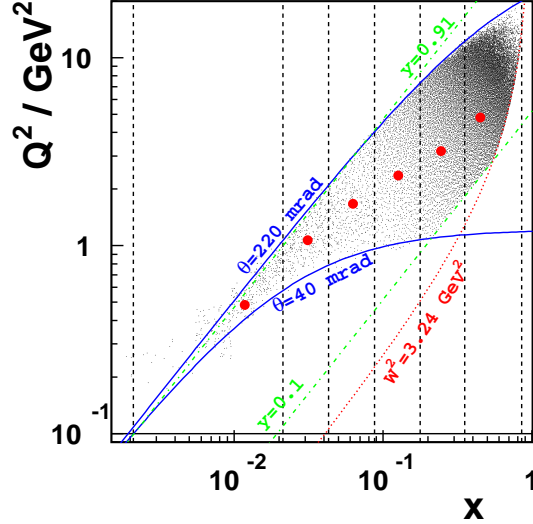
Figure 3: Kinematic coverage of the HERMES measurement. The dashed vertical lines indicate the borders of the bins in x, the dots their centers of gravity. The solid curves indicate the vertical acceptance of the spectrometer, defined by its aperture. In addition, the kinematic cuts imposed on the variables Q^2, y and W^2 are shown. *Reproduced from [9].*

are roughly within two sigma from zero, which calls for a higher precision measurement. Another issue is that some of the HERMES momentum transfer values are low (see Fig. 3), so that quark structure functions may not be the correct language. The Q^2 variation in each x-bin is also quite wide ($\approx$10 GeV^2 for $x \sim 0.3$), which complicates the interpretation of this data, since several models predict significant Q^2-dependence of b_1. See for example Fig. 4.

1.3   The Tensor Structure Function $b_1(x)$

The leading twist tensor structure function b_1 quantifies effects not present in the case of spin-1/2 hadrons. However, tensor effects only exist in nuclear targets, so the study of b_1 serves as a very interesting bridge between nucleon and nuclear physics. On the one hand, deep inelastic scattering (DIS), clearly probes partonic degrees of freedom, i.e. quarks, but on the other hand, b_1 depends solely on the deuteron (nuclear) spin state as seen in Eq. 11. We discuss now several predictions for the x dependence of b_1.

1.3.1   Conventional Nuclear Effects

In Ref. [8], the authors note that $b_1(x)$ is small and calculable for a weakly bound system like the deuteron, and that its measurement would provide a clear signature for exotic components in a spin one nucleus. In effect, $b_1(x)$ measures the extent to which a target nucleus deviates from a trivial bound state of protons and neutrons. The authors evaluate the value of b_1 in three conventional

12

scenarios for the deuteron constituents and their dynamics:

I. If the deuteron is composed of two spin-1/2 non-interacting nucleons at rest, then the eight helicity amplitudes characteristic of a spin-1 target are expressed in terms of the four helicity amplitudes of each spin-1/2 nucleons, and therefore the total number of independent amplitudes is reduced from eight to four. All structure functions of the deuteron are then the simple sum of the structure functions of the two nucleons, and the tensor structure functions vanish: $b_1 = b_2 = b_3 = b_4 = 0$.

II. If instead, the deuteron is composed of two spin-1/2 nucleons moving non-relativistically in a central potential, then the target motion modifies the helicity amplitudes. Using the convolution formalism, it was found that the contribution of these moving nucleons to b_1 is small and is dominated by the lower component of the nucleon's Dirac wave function.

III. In the final scenario considered, the deuteron contains a D-state admixture. Because the proton and the neutron are moving in opposite directions, an additional term due to the $S - D$ interference appears in the convolution procedure. This extra contribution to b_1 is predicted to be even smaller than in the previous case.

All three scenarios predict a small or vanishing b_1, leading the authors to predict that $b_1 \approx 0$ for the deuteron.

As an interesting counter example for which b_1 could be significant, the authors consider a model of a massless relativistic quark with $j = 3/2$ moving in a central potential. In this calculation, a meson in the $j = 1$ state is formed from the coupling of a $P_{3/2}$ massless quark with a spin-1/2 spectator. This crude model predicts that $b_1(x)$ exhibits large negative values peaked around $x = 0.5$ [8]. Curiously, this behavior is possibly mirrored by the existing HERMES data (see Fig. 4), but there is only a single data point with large uncertainty in this region.

1.3.2 Nuclear Pions

In 1988, Miller also examined the tensor structure function b_1 [14]. The basic mechanism is that the virtual photon hits an exchanged pion which is responsible for the binding of the deuteron. In this early calculation, the convention used by Miller for b_1 was different from that used in the HERMES results and in Ref. [13]. A recent update to this calculation [15], which uses a consistent convention and the pion structure function from [16], is shown in Fig. 4. The spread of the curve originates from the parameter $A_s = (.9 \pm 0.3)$ which governs the strength of the sea in the pion. Miller's calculation, similar to other 'non-exotic' models, is unable to reproduce the trend of the HERMES data, and predicts very small values of $b_1(x)$ at intermediate and large x.

1.3.3 Convolution Model

Khan and Hoodbhoy [1] evaluated $b_1(x)$ in a convolution model with relativistic and binding energy corrections. They use this to evaluate the effect of nuclear Fermi motion and binding on the deuteron structure functions. They observe that for zero Fermi motion and binding $b_1^D(x) = 0$. They also predict a small enhancement of b_1 in the region of $x \sim 0.3$, as seen in Fig. 5. Note
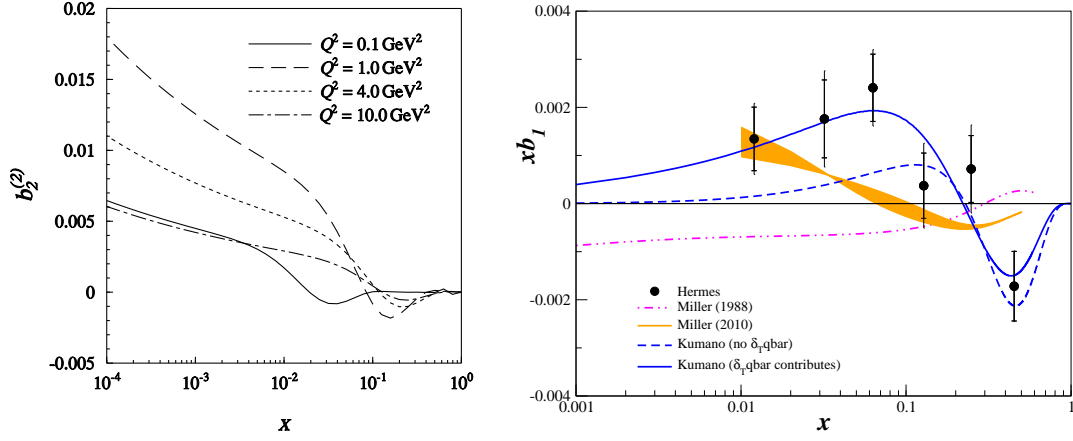
Figure 4: Theoretical predictions. **Left plot:** Double-scattering contribution to $b_2(x, Q^2)$ as a function of x [12]. Note the strong Q^2 dependence at low x. **Right plot:** HERMES results [10] compared to calculations from S. Kumano [13] and from the one-pion exchange effects of G. Miller [14, 15].

Figure 5: Prediction for $b_1^D(x)$ (solid curve) from Ref. [1], the S-D contribution to $b_1^D(x)$ (dashed curve), and the D-D contribution to $b_1^D(x)$ (dot-dashed curve). Note the vertical scale which would make the curve mostly indiscernible from zero in Fig. 4 (right). *Reproduced from Ref. [1].*

14

Figure 6: Relativistic convolution calculation of $b_1^D(x)$ and $b_2^D(x)$. Curves: BS - solid, Bonn - dotted, Bonn with cut -dashed. *Reproduced from Ref. [17].*
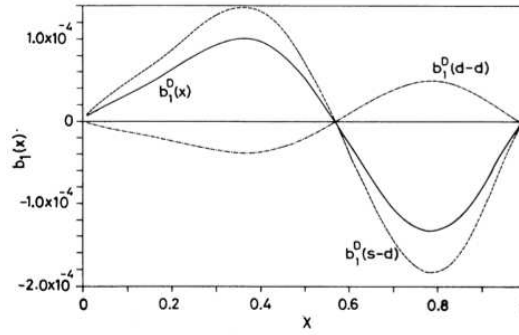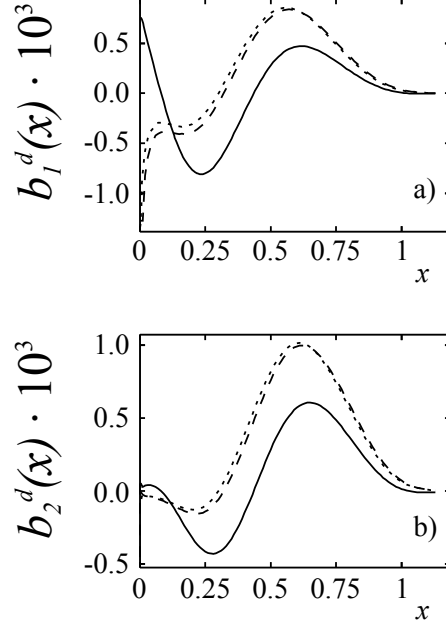
however, that the absolute scale of this predicted b_1 is $\mathcal{O}(10^{-4})$, while the HERMES data implies that the scale is more than an order of magnitude larger than this.

1.3.4 Relativistic Calculation

Umnikov [17] calculated $b_1(x)$ and $b_2(x)$ within a covariant approach, based on the relativistic convolution formalism for DIS and the Bethe-Salpeter formalism for the deuteron bound state. Fig. 6 sets the scale for $b_1(x)$ at the 10^{-3} level. Both the relativistic and non-relativistic calculations are consistent with the CK sum rule (see Sec. 1.3.8), although the nonrelativistic convolution model results in an incorrect behavior of at low x.

1.3.5 Double-Scattering Effects

Using Vector Meson Dominance (VMD), the authors of Ref. [12] isolate the double-scattering contribution to b_1. The existence time of a vector meson can be described by the coherence length:

$$\lambda = \frac{Q^2}{Mx(M_v^2 + Q^2)} \tag{13}$$

which is the length over which the vector meson propagates during the time $\Delta t = 1/\Delta E$. For significant shadowing or double scattering to occur, a minimum coherence length of ≈ 1.7 fm (the inter-nucleon separation) is required. At $x > 0.3$, the coherence length is only about the

size of the nucleon, so double scattering contributions are anticipated to be negligible. However, for $x \leq 0.1$, double-scattering should be significant in b_1 behaving as $(1-x)^{2\delta}/x^{1+2\delta}$, where δ is determined from the soft pomeron intercept $\alpha_P(t=0) = 1 + \delta$. The authors predicted a significant enhancement of b_1 at low x (≤ 0.01) due to the quadrupole deformation of the deuteron, which is qualitatively confirmed by the HERMES data. See Fig. 2.

1.3.6 Virtual Nucleon Approximation

M. Sargsian [18] recently calculated the tensor asymmetry A_{zz} for deep inelastic scattering. See Fig. 7. In the approximation in which only proton-neutron component of the deuteron is taken into account and nuclear parton distributions are generated through the convolution of partonic distribution of nucleon and deuteron density matrix (see e.g. Refs. [19, 20]), the deuteron structure function b_1 is related directly to the d-partial wave of the deuteron wave function [18, 19]. As a result, this approximation predicts negligible magnitude for b_1 for $x \leq 0.6$ due to small Fermi momenta involved in the convolution integral. However, the predicted magnitude of b_1 is large at $x \geq 0.7$ where one expects substantial contribution from the d-waves due to high momentum component of the deuteron wave function involved in the convolution picture of DIS scattering off the deuteron. In this case, b_1 is very sensitive to the relativistic description of the deuteron and its measurement can be used for checking the different approximations of high momentum component of deuteron wave function.

In the calculation presented, two Virtual Nucleon and Light-Cone approximations are used to calculate the tensor polarization for DIS scattering off the deuteron. In both approximations only the proton-neutron component of the deuteron is taken into account. In the Virtual Nucleon approximation, the covariant scattering amplitude is reduced by estimating the spectator nucleon propagator at its on-energy shell in the lab frame of the deuteron. Within this approximation the baryonic sum rule is satisfied while the momentum sum rule is not. The latter is due to the fact that part of the light cone momentum of the bound virtual nucleon is lost to the unaccounted non-nucleonic degrees of freedom in the deuteron wave function. In the light cone approximation the scattering amplitude is estimated the $E + p_z$ pole of the spectator nucleon on the light cone. In this case the wave function is defined on the light-cone reference frame and it satisfies both baryon number and momentum sum rules. For the detailed comparison of these approximations, see Ref. [20].

1.3.7 Fit to HERMES Data

Kumano [13] points out that the twist-2 structure functions b_1 and b_2 can be used to probe orbital angular momentum. He then extracts the tensor polarized quark and anti-quark distributions from a fit to the HERMES data [10]. He finds that a non-negligible tensor polarization of the sea is necessary to reproduce the trend of the data, as shown in Fig. 4. However, this conclusion has to be considered with caution due to the extended Q^2 coverage (Fig. 3), and large uncertainty of each HERMES data point. In particular, the author calls for better measurements of b_1 at large x (> 0.2), and further investigation of the tensor structure functions in general.

1.3.8 The Close-Kumano Sum Rule

Following the formalism from the parton model in [8], Close and Kumano [21] related the tensor structure function b_1 to the electric quadrupole form factor of the spin-1 target through a sum rule[§]:

$$
\begin{aligned}
\int_0^1 dx\, b_1(x) &= -\frac{5}{12M^2} \lim_{t \to 0} t\, F_Q(t) + \frac{1}{9}\big(\delta Q + \delta \bar{Q}\big)_s \\
&= \frac{1}{9}\big(\delta Q + \delta \bar{Q}\big)_s = 0
\end{aligned}
\tag{14}
$$

where $F_Q(t)$ is the electric quadrupole form factor of a spin-1 hadron at the momentum squared t. The Close Kumano (CK) sum rule is satisfied in the case of an unpolarized sea. The authors note that in nucleon-only models, the integral of b_1 is not sensitive to the tensor-polarization of the sea, and consequently the sum rule is always true, even when the deuteron is in a D-state.

The authors of Ref. [1] calculated the first moment of $b_1(x)$ in a version of the convolution model that incorporates relativistic and binding energy corrections. They found a value of $-6.65 \cdot 10^{-4}$, and emphasize that deviations from this will serve as a good signature of exotic effects in the deuteron wave function. Similarly, Ref. [17] predicts $5 \cdot 10^{-4}$ and $3 \cdot 10^{-5}$ for the relativistic and nonrelativistic calculation of Eq. 14, respectively.

A truncated version of Eq. 14 was evaluated by the HERMES [9, 10] experiment and found to be:

$$
\int_{0.0002}^{0.85} b_1(x)dx = 0.0105 \pm 0.0034 \pm 0.0035
\tag{15}
$$

which possibly indicates a breaking of the Close-Kumano sum rule, and consequently a tensor-polarized quark sea. However, since the comparison is only at the two sigma level, more precise data is needed for a true test.

1.3.9 Angular Momentum Sum Rule for Spin-1 Hadronic Systems

The b_1 structure function is connected with the spin-1 angular momentum sum rule as discussed in Ref. [2]. By examining the energy momentum tensor for the deuteron, the authors showed that it was possible to define an additional sum rule for b_1 (see Eq. 12 in Ref. [2]) where it was shown that the second moment of this quantity is non vanishing, being related to one of the gravitomagnetic deuteron form factors. A measurement of b_1 would provide a unique test of this idea.

It is also important to notice that b_1 singles out the role of the D-wave component in distinguishing coherent nuclear effects through tensor polarized correlations from the independent nucleon's partonic spin structure. A similar role of the D-wave component was also found in the recently proposed spin sum rule where it plays a non-trivial role producing a most striking effect through the spin flip GPD E. An experimental measurement of b_1 would corroborate this scenario.

[§]Efremov and Teryaev evidently proposed the same relation for mesons in Ref. [22].

1.4 Interest from Theorists

During the preparation of this proposal, we contacted several theorists to gauge interest in a precision measurement of b_1. The response was uniformly positive. We provide some of their feedback for context.

It is known that b_1 is sensitive to dynamical aspects of constituents with angular momenta. Measurements of b_1 could open a new field of spin physics because this kind of spin physics has not been explored anywhere else. The only experimental information came from the HERMES collaboration; however, their data are not accurate enough to find the x dependence of b_1, especially at large x.

It is an unique opportunity at JLab to develop this new field of spin physics.

S. Kumano (KEK)

I'm glad to hear that b_1 is not forgotten in all the excitement about other spin dependent effects.

R. Jaffe (MIT)

I am particularly interested in signatures of novel QCD effects in the deuteron. The tensor charge could be sensitive to hidden color [23, 24] (non-nucleonic) degrees of freedom at large x. It is also interesting that antishadowing in DIS in nuclei is not universal but depends on the quark flavor and spin. One can use counting rules from PQCD to predict the $x \rightarrow 1$ dependence of the tensor structure function.

S. Brodsky (SLAC)

I am certainly interested in the experimental development to find the novel QCD phenomena from the hidden color component of deuteron.

Chueng-Ryong Ji (NCSU)

You have finally piqued my interest in this subject...Surely this is of real interest the spin community! I hope I might be able to say something coherent about the partonic interpretation at some point– this of course is where my real interest lays.

Leonard Gamberg (Penn State Berks)

I find the proposal well written, well justified, sound, and exciting.

Alessandro Bacchetta (Universita di Pavia)

	$\overline{x}$	$\overline{Q^2}$	$\overline{W}$	P_0	θ	Rates	time
		(GeV^2)	(GeV)	(GeV)	(deg.)	(kHz)	(days)
SHMS	0.15	1.21	2.78	6.70	7.35	1.66	6
SHMS	0.30	2.00	2.36	7.45	8.96	0.79	9
SHMS	0.452	2.58	2.00	7.96	9.85	0.38	15
HMS	0.55	3.81	2.00	7.31	12.50	0.11	30

Table 1: Summary of the kinematics and physics rates using the Hall C spectrometers.

$\overline{x}$	$\overline{Q^2}$	$\overline{W}$	δA_{zz}^{stat}	δb_1^{stat}
	(GeV^2)	(GeV)	$\times 10^{-2}$	$\times 10^{-2}$
0.16	1.17	2.65	0.15	0.18
0.28	1.76	2.35	0.39	0.28
0.36	2.12	2.16	0.50	0.23
0.49	3.25	2.07	0.37	0.08

Table 2: Summary of the expected statistical uncertainty after combining overlapping x-bins. Values represent the statistics weighted average of all events that satisfy our DIS cut.

2 The Proposed Experiment

We will measure the leading twist tensor structure function b_1 via the tensor asymmetry A_{zz} for $0.16 < x < 0.49$, $0.8 < Q^2 < 5.0$ GeV^2 and $W \geq 1.85$ GeV. Figs. 8 and 9 shows the planned kinematic coverage utilizing the Hall C HMS and SHMS spectrometers at forward angle.

The polarized ND$_3$ target is discussed in section 2.2. The magnetic field of the target will be held constant along the beamline at all times, while the target state is alternated between a polarized and unpolarized state. The tensor polarization, packing fraction and dilution factor used in the rates estimate are 20%, 0.65 and 0.285 respectively. With an incident electron beam current of 115 nA, the expected deuteron luminosity is 1.57×10^{35} / cm$^2 \cdot$s^1. The momentum bite and the acceptance were assumed to be $\Delta P = \pm 8\%$ and $\Delta \Omega = 5.6$ msr for the HMS, and $\Delta P = ^{+20\%}_{-8\%}$ and $\Delta \Omega = 4.4$ msr for the SHMS. For the choice of the kinematics, special attention was taken onto the angular and momentum limits of the spectrometers: for the HMS, $10.5° \leq \theta \leq 85°$ and $1 \leq P_0 \leq 7.3$ GeV/c, and for the SHMS, $5.5° \leq \theta \leq 40°$ and $2 \leq P_0 \leq 11$ GeV/c. In addition, the opening angle between the spectrometers is physically constrained to be larger than 17.5°. The invariant mass W was kept to $W \geq 1.85$ GeV for all settings. The projected uncertainties for A_{zz} and b_1 are summarized in Table 2, and displayed in Fig. 7.

A total of 30 days of beam time is requested for production data, with an additional 10.8 days of expected overhead.
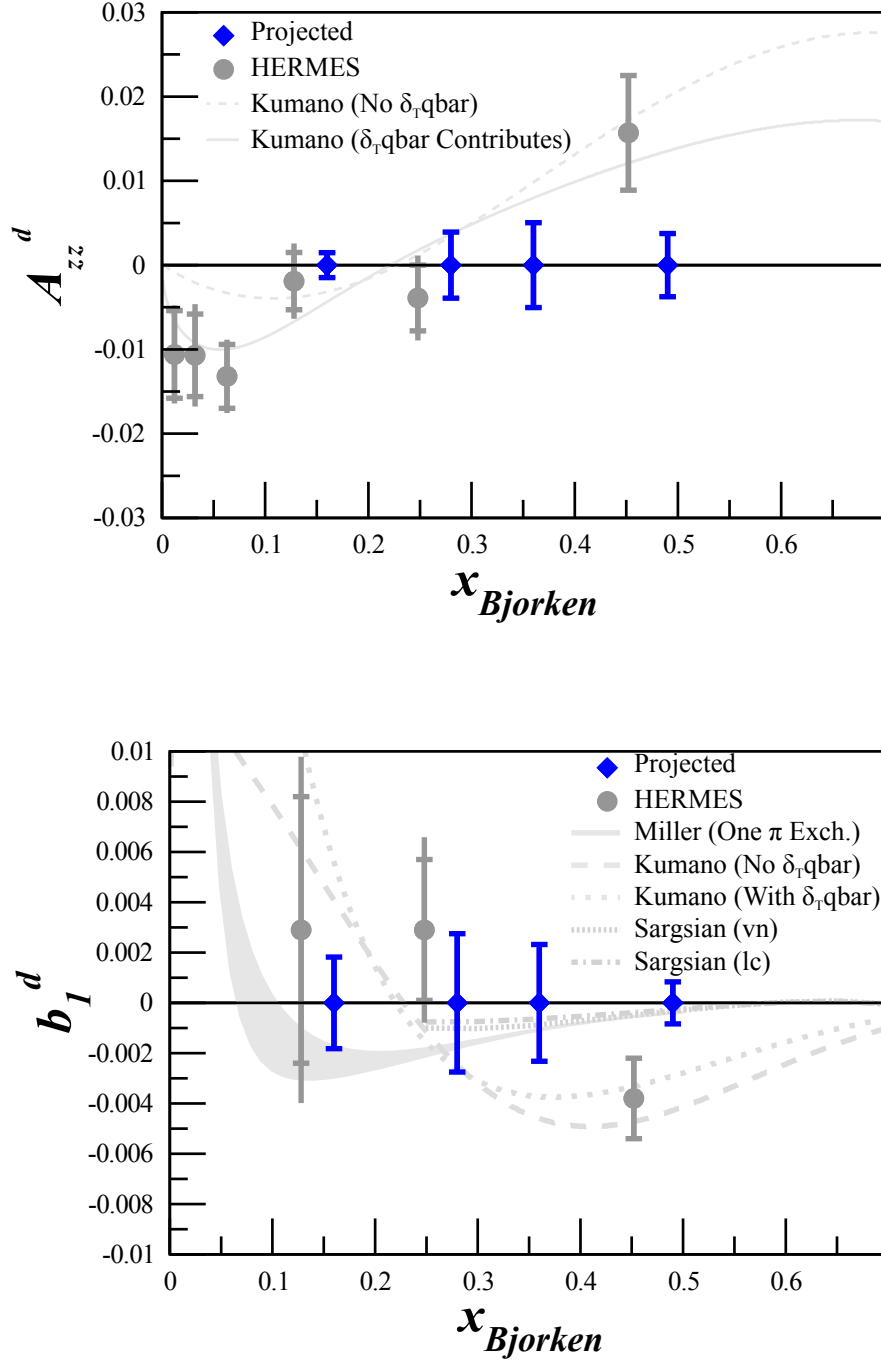
Figure 7: **Top:** Projected statistical errors for the tensor asymmetry A_{zz} with 30 days of beam time. **Bottom:** Projected statistical errors for the tensor structure function b_1. Data at different Q^2 are combined with an x-binning that varies slightly per point, but is approximately ± 0.05. Also shown are the HERMES data [10], and the calculations from Kumano [13], Miller [14, 15], and Sargsian [18].

Figure 8: Kinematic coverage. The grey settings are not included in our rates estimates since they fall below $W \geq 1.85$GeV. The points labeled *Input* represent the central value of the spectrometer setting, which are not the statistics weighted average of the distribution.
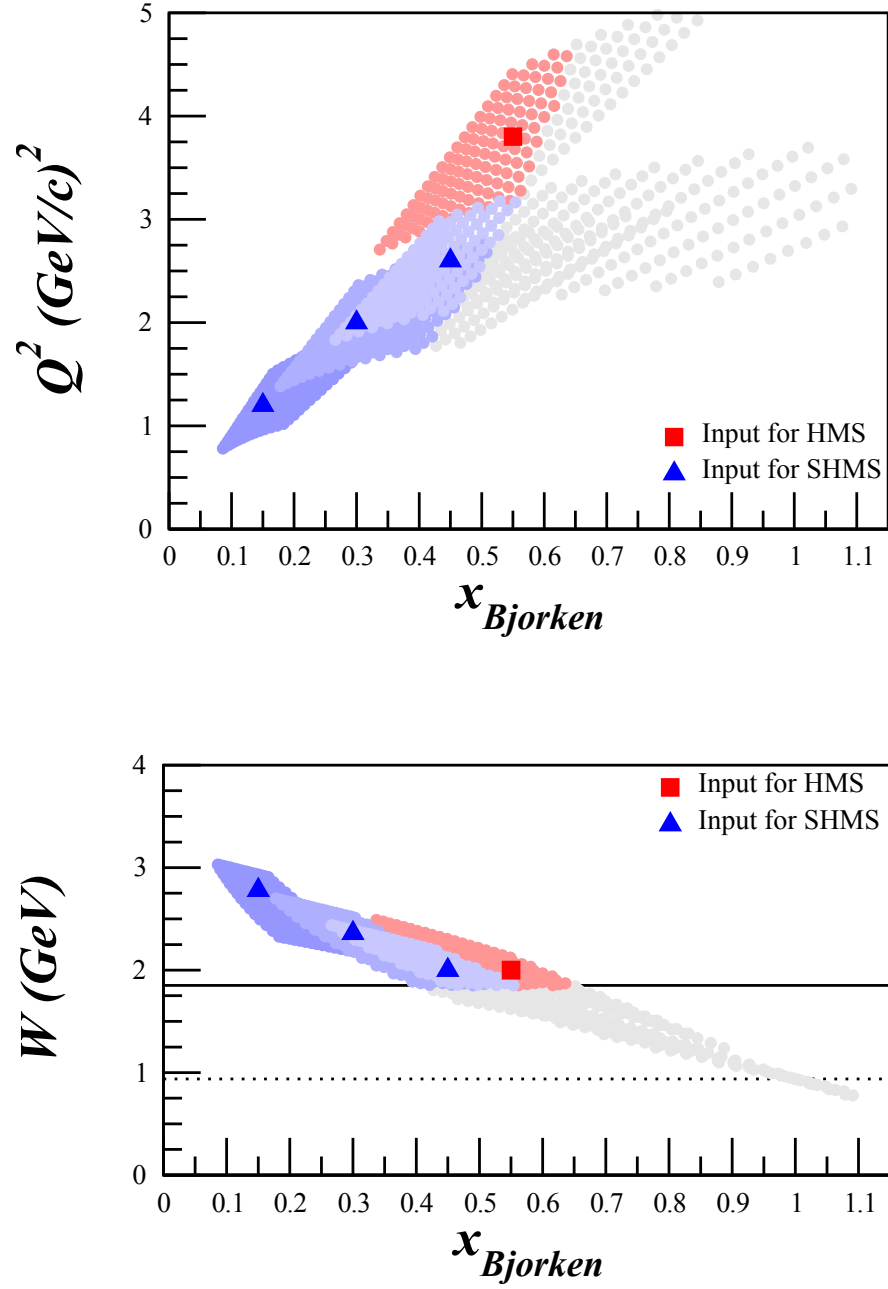
Figure 9: Kinematic coverage. The grey settings are not included in our rates estimates since they fall below $W \geq 1.85$GeV. The points labeled *Input* represent the central value of the spectrometer setting, which are not the statistics weighted average of the distribution.
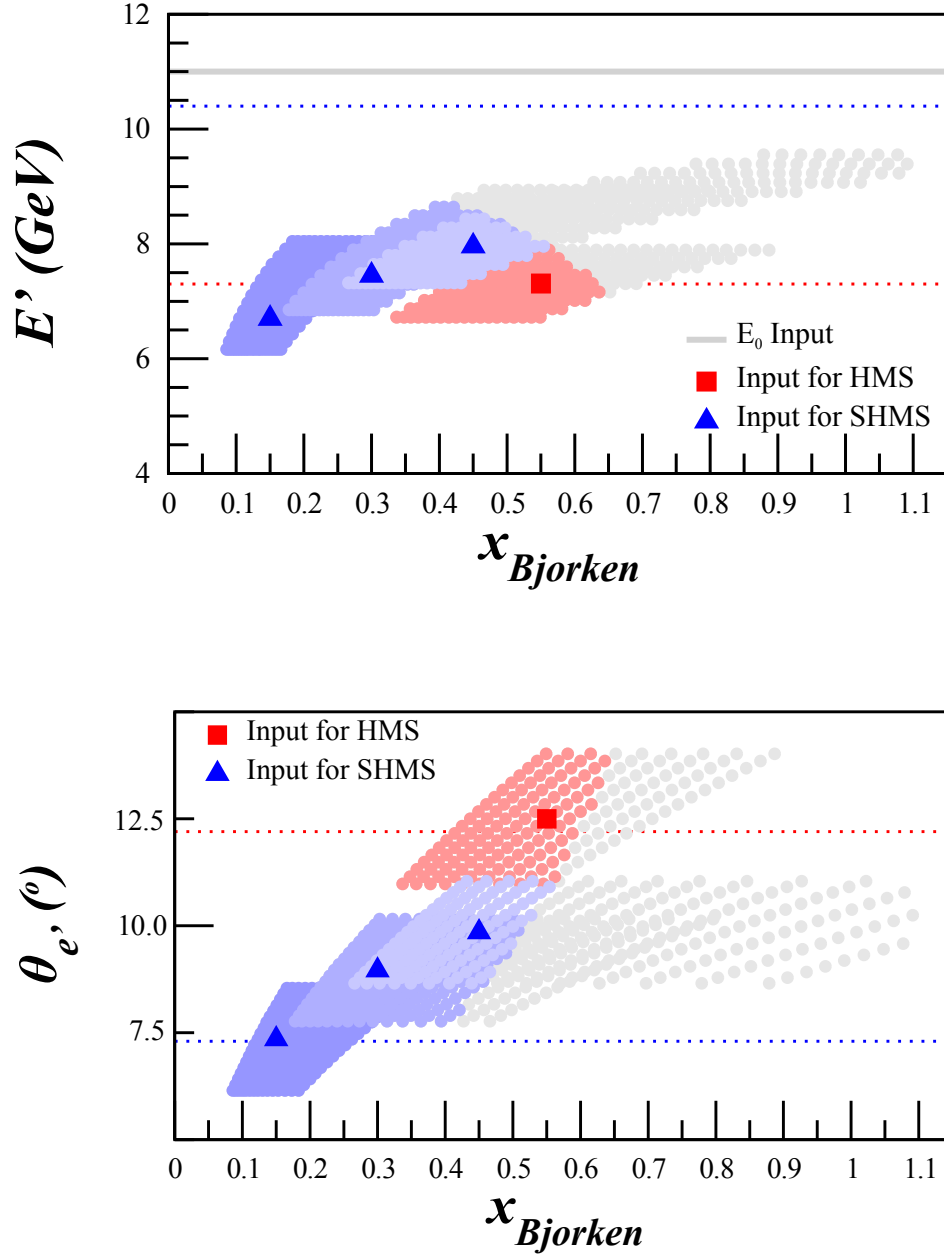
2.1 Experimental Method

The measured DIS double differential cross section for a spin-1 target characterized by a vector polarization P_z and tensor polarization P_{zz} is expressed as,

$$\frac{d^2\sigma_p}{dxdQ^2} = \frac{d^2\sigma}{dxdQ^2}\left(1 - P_z P_B A_1 + \frac{1}{2}P_{zz}A_{zz}\right), \tag{16}$$

where, σ_p (σ) is the polarized (unpolarized) cross section, P_B is the incident electron beam polarization, and A_1 (A_{zz}) is the vector (tensor) asymmetry of the virtual-photon deuteron cross section. This allows us to write the positive polarized tensor, $0 < P_{zz} \le 1$, asymmetry using unpolarized electron beam as,

$$A_{zz} = \frac{2}{P_{zz}}\left(\frac{\sigma_1}{\sigma} - 1\right) \tag{17}$$

where σ_1 is the polarized cross section for

$$P_{zz} = \frac{n_+ - 2n_0 + n_-}{n_+ + n_- + n_0}, \text{ for } n_+ + n_- > 2n_0. \tag{18}$$

Here n_m represents the portion of the ensemble in the m state.

Eq. 17 reveals that the asymmetry A_{zz} compares two different cross sections measured under different polarization conditions of the target, positively tensor polarized and unpolarized. To obtain the relative cross section measurement in the same configuration, the same target cup and material will be used at alternating polarization states (polarized vs. unpolarized), and the magnetic field providing the quantization axis will be oriented along the beamline at all times. This field will always be held at the same value, regardless of the target material polarization state. This ensures that the acceptance remains consistent within the stability (10^{-4}) of the super conducting magnet.

Since many of the factors involved in the cross sections cancel in the ratio, Eq. 17 can be expressed in terms of the charge normalized, efficiency corrected numbers of tensor polarized N_1^c and unpolarized N^c counts,

$$A_{zz} = \frac{2}{fP_{zz}}\left(\frac{N_1^c}{N^c} - 1\right) \tag{19}$$

The dilution factor f corrects for the presence of unpolarized nuclei in the target.

The measured tensor asymmetry allows for an extraction of the tensor structure function b_1 using the world data on the leading-twist structure function F_1^d,

$$b_1 = -\frac{3}{2}F_1^d A_{zz} \tag{20}$$

In Eq. 19, the dilution factor is defined as,

$$f = \frac{N_D \sigma_D}{N_N \sigma_N + N_D \sigma_D + \Sigma N_A \sigma_A}, \tag{21}$$

23

where N_D is the number of deuterium nuclei in the target and σ_D is the corresponding inclusive double differential scattering cross section, N_N is the nitrogen number of scattered nuclei with cross section σ_N, and N_A is the numbers of other scattering nuclei of mass number A with cross section σ_A. The denominator of the dilution factor can be written in terms of the relative volume ratio of ND_3 to LHe in the target cell, otherwise known as the packing fraction p_f. In our case of a cylindrical target cell oriented along the magnetic field, the packing fraction is exactly equivalent to the percentage of the cell length filled with ND_3. The dilution factor is discussed in further detail in Sec. 2.2.3.

The time necessary to achieve the desired precision δA is:

$$T = \frac{N_T}{R_T} = \frac{16}{P_{zz}^2 f^2 \delta A_{zz}^2 R_T} \tag{22}$$

where R_T is the total rate and $N_T = N^1 + N$ is the total estimated number of counts to achieve the uncertainty δA_{zz}.

2.1.1 Statistical Uncertainty

To investigate the statistical uncertainty we start with the equation for A_{zz} using measured counts for polarized data N_1 and unpolarized data N,

$$A_{zz} = \frac{2}{f P_{zz}} \left(\frac{N_1}{N} - 1 \right). \tag{23}$$

The absolute error with respect to counts in then,

$$\delta A_{zz} = \frac{2}{f P_{zz}} \sqrt{\left(\frac{\delta N_1}{N} \right)^2 + \left(\frac{N_1 \delta N}{N^2} \right)^2}. \tag{24}$$

For small asymmetries, $N_1 \approx N$, so that twice N is required to obtain the total number of counts N_T for the experiment. This leads to:

$$\delta A_{zz} = \frac{4}{f P_{zz}} \frac{1}{\sqrt{N_T}}. \tag{25}$$

2.1.2 Systematic Uncertainty

Table 3 shows a list of the scale dependent uncertainties contributing to the systematic error in A_{zz}. With careful minimization, the uncertainty in P_z can be held to better than 4%, as demonstrated in the recent g2p/GEp experiment [25]. This leads to a a relative uncertainty in P_{zz} of 7.7%. Alternatively, the tensor asymmetry can be directly extracted from the NMR lineshape as discussed in Sec. 2.2, with similar uncertainty. The uncertainty from the dilution factor and packing fraction of the ammonia target contributes at the 4% level. The systematic effect on A_{zz} due to the QED radiative corrections will be quite small. For our measurement there will be no polarized radiative corrections at the lepton vertex, and the unpolarized corrections are known to better than 1.5%. Charge calibration and detector efficiencies are expected to be known better to 1%, but the impact of time-dependent drifts in these quantities must be carefully controlled.

Source	Systematic
Polarimetry	8.0%
Dilution/packing fraction	4.0%
Radiative corrections	1.5%
Charge Determination	1.0%
Detector resolution and efficiency	1.0%
Total	9.2%

Table 3: Estimates of the scale dependent contributions to the systematic error of A_{zz}.

Time dependent factors

Eq. 19 involves the ratio of counts, which leads to cancellation of several first order systematic effects. However, the fact that the two data sets will not be taken simultaneously leads to a sensitivity to time dependent variations which will need to be carefully monitored and suppressed. To investigate the systematic differences in the time dependent components of the integrated counts, we need to consider the effects from calibration, efficiency, acceptance, and luminosity between the two polarization states.

In order to look at the effect on A_{zz} due to drifts in beam current measurement calibration and detector efficiency, we rewrite Eq. 19 explicitly in terms of the raw measured counts N_1 and N,

$$
\begin{aligned}
A_{zz} &= \frac{2}{fP_{zz}}\left(\frac{N_1^c}{N^c}-1\right) \\
&= \frac{2}{fP_{zz}}\left(\frac{Q\varepsilon l\mathcal{A}}{Q_1\varepsilon_1 l\mathcal{A}}\frac{N^1}{N}-1\right)
\end{aligned}
\tag{26}
$$

where Q represents the accumulated charge, and ε is the detector efficiency. The target length l and acceptance $\mathcal{A}$ are identical in both states, to first order.

We can then express Q_1 as the change in beam current measurement calibration that occurs in the time it takes to collect data in one polarization state before switching such that $Q_1 = Q(1-\delta Q)$. In this notation, δQ is a dimensionless ratio of charges in the different polarization states. A similar representation is used for drifts in detector efficiency leading to,

$$
A_{zz} = \frac{2}{fP_{zz}}\left(\frac{N_1 Q(1-\delta Q)\varepsilon(1-\delta\varepsilon)}{NQ\varepsilon}-1\right).
\tag{27}
$$

which leads to,

$$
A_{zz} = \frac{2}{fP_{zz}}\left(\frac{N_1}{N}(1-\delta Q-\delta\varepsilon+\delta Q\delta\varepsilon)-1\right).
\tag{28}
$$

We can obtain estimates of δQ and $\delta\varepsilon$ from previous experiments. For the HRS detector drift during the JLab transversity experiment E06-010, the detector response was measured such that the normalized yield for the same condition over a three month period indicated little change ($< 1\%$). These measurements indicated that for the short time (20 minutes) between target spin flips, the

25

detector drift should be less than 1% times the ratio of the time period between target spin flips and three months.

For the present proposal, we use the same estimate except that the period between target polarization states is $\approx$12 hours leading to an overall drift $\delta\varepsilon \sim 0.01\%$. A similar approach can be used to establish an estimate for δQ using studies from the data from the (g2p/GEp) experiment, resulting in $\delta Q \sim 0.01\%$.

To express A_{zz} in terms of the estimated experimental drifts in efficiency and current measurement we can write,

$$A_{zz} = \frac{2}{fP_{zz}}\left(\frac{N_1}{N} - 1\right) \pm \frac{2}{fP_{zz}}\delta\xi. \tag{29}$$

where $\delta\xi = \delta Q + \delta\varepsilon$. This leads to a contribution to A_{zz} on the order of 1×10^{-3},

$$dA_{zz}^{drift} = \pm\frac{2}{fP_{zz}}\delta\xi = \pm 3.7 \times 10^{-3}. \tag{30}$$

The polarization state of the target will be changed every 12 hours, so each of our settings will involve between $N = 12$ to $N = 60$ polarization cycle pairs. This further suppreses the effect of any drift to less than the 10^{-3} level. Though a very important contribution to the error, this value allows a clean measurement of $A_{zz} = 0$ at $x = 0.45$ without overlap with the Hermes error bar. For this estimate we assumed only two polarization state changes in a day. Increasing this rate decreases the systematic effect in A_{zz} accordingly, but at the cost of increased overhead.

Detector efficiencies can drift for a variety of reasons, including fluctuations in gas quality, high voltage drift, or drifts in the spectrometer magnetic fields. All of these types of variation can be controlled and minimized during the experiment through careful monitoring as well as systematic studies of the data collected.

The identical configuration of the two polarization states minimizes the relative changes in luminosity with respect to time. Consistency checks on the measured cross section data can be implemented to ensure the quality of each run used in the asymmetry analysis. Fluctuations in luminosity due to target density variation can be kept to a minimum by keeping the material beads at the same temperature for both polarization states through control of the microwave and the LHe evaporation. The He vapor pressure reading provides an accuracy of material temperature changes at the level of $\sim$0.1%. Beam rastering can also be controlled to a high degree.

The dominant source of any variation in acceptance $\mathcal{A}$ from state to state will be the stability of the target magnetic field. The capacity to set and hold the target super conducting magnet to a desired holding field is $\delta B/B = 0.01\%$. The same target cup will be used for each state, which removes any variation in the target length l.

2.1.3 Overhead

Table 4 summarizes the expected overhead, which sums to 10.8 days. The dominant overhead comes from switching from the polarized to unpolarized state and vice versa. Target anneals will need to be performed about every other day, and the material replaced once a week. Measurements of the dilution from the unpolarized materials contained in the target, and of the packing fraction due to the granular composition of the target material will be performed with a carbon target.

Overhead	Number	Time Per (hr)	(hr)
Polarization/depolarization	60	2.0	120.0
Target anneal	13	4.0	52.0
Target T.E. measurement	5	4.0	20.0
Target material change	4	4.0	16.0
Packing Fraction/Dilution runs	6	1.0	6.0
BCM calibration	8	2.0	16.0
Optics	3	4.0	12.0
Linac change	1	8.0	8.0
Momentum/angle change	3	2.0	6.0
			10.8 days

Table 4: Contributions to the experimental overhead.

2.2 Polarized Target

This experiment will use the JLab/UVa dynamically polarized solid ND_3 target operated in longitudinal mode. The target is typically operated with a specialized slow raster, and beamline instrumentation capable of characterizing the low current 50-115 nA beam. All of these requirements have been met previously in Hall C. The polarized target (see Fig. 10), has been successfully used in experiments E143, E155, and E155x at SLAC, and E93-026, E01-006 and E07-003, E08-027 and E08-007 at JLab. A similar target was used in Hall B for the EG1,EG4 and DVCS experiments.

The JLab/UVa target underwent significant renovation and improvement [26] during the recent g2p run. The magnet was replaced early in the run, and the target then performed consistently at or above historical levels. A new 1 K refrigerator and target insert were designed and constructed by the JLab target group. The cryogenic pumping system has been overhauled. In particular, the older Alcatel 2060H rotary vane pumps have been replaced with new Pfeiffer DU065 magnetically coupled rotary vane pumps, and the pump controls are being refurbished. The target motion system has been rebuilt from scratch.

The target operates on the principle of Dynamic Nuclear Polarization, to enhance the low temperature (1 K), high magnetic field (5 T) polarization of solid materials by microwave pumping. The polarized target assembly contains several target cells of 3.0 cm length that can be selected individually by remote control to be located in the uniform field region of a superconducting Helmholtz pair. The permeable target cells are immersed in a vessel filled with liquid Helium and maintained at 1 K by use of a high power evaporation refrigerator. The coils have a $50°$ conical shaped aperture along the beam axis which allow for unobstructed forward scattering.

The target material is exposed to microwaves to drive the hyperfine transition which aligns the nucleon spins. The heating of the target by the beam causes a drop of a few percent in the polarization, and the polarization slowly decreases with time due to radiation damage. Most of the radiation damage can be repaired by periodically annealing the target, until the accumulated dose reached is greater than about 0.5×10^{17} e$^-$/cm^2, at which time the target material needs to be replaced.
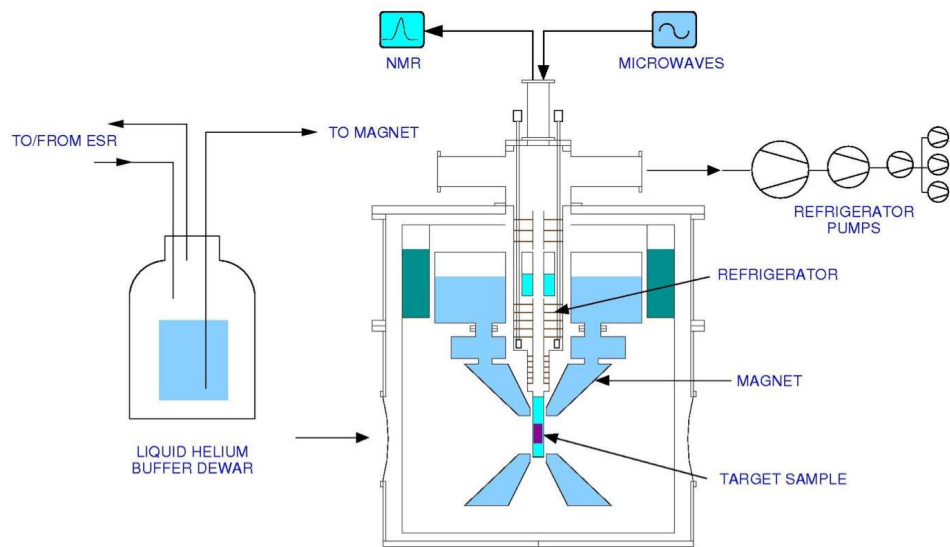
Figure 10: Cross section view of the JLab/UVa polarized target. Figure courtesy of C. Keith.
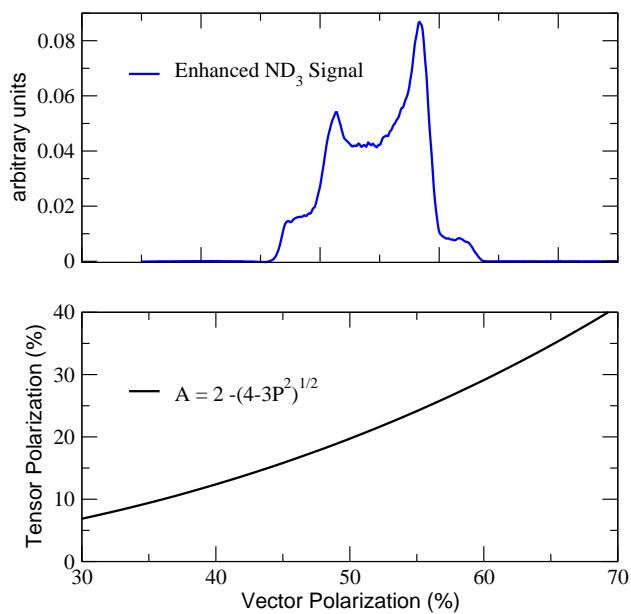

Figure 11: **Top**: NMR signal for ND_3 with a vector polarization of approximately 50% from the GEN experiment. **Bottom**: Relationship between vector and tensor polarization in equilibrium, and neglecting the small quadrupole interaction.
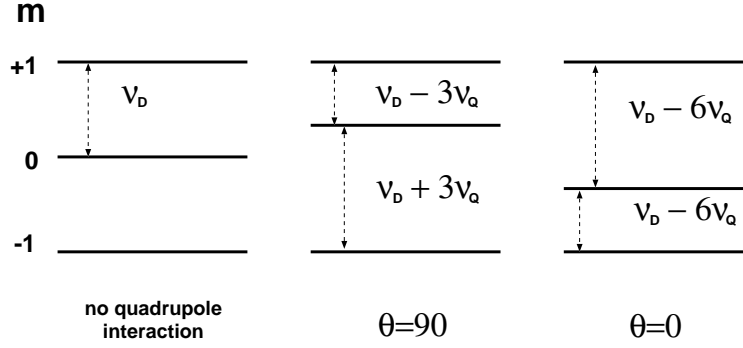
Figure 12: Energy levels in ND$_3$. The level spacing is shifted by the quadrupole interaction, which depends on the angle θ between the magnetic field and the electric field gradient.

2.2.1 Polarization Analysis

The three Zeeman sublevels of the deuteron system ($m = -1, 0, 1$) are shifted unevenly due to the quadrupole interaction [3]. This shift depends on the angle between the magnetic field and the electrical field gradient, and gives rise to two separate transition energies. Hence, the unique double peaked response displayed in Fig. 11.

The energies [27] of these three magnetic sublevels are:

$$E = -h\nu_D m + h\nu_Q \left[(3\cos^2(\theta) - 1) \right] \left[3m^2 - I(I+1) \right] \tag{31}$$

where ν_D is the deuteron Larmor frequency and ν_Q is a function of the deuteron quadrupole moment eQ. The quadrupole interaction shifts these levels depending on the angle θ between the magnetic field and the electrical field gradient, as shown in Fig. 12.

When the system is at thermal equilibrium with the solid lattice, the deuteron polarization is known from:

$$P_z = \frac{4 + \tanh \frac{\mu B}{2kT}}{3 + \tanh^2 \frac{\mu B}{2kT}} \tag{32}$$

where μ is the magnetic moment, and k is Boltzmann's constant. The vector polarization can be determined by comparing the enhanced signal with that of the TE signal (which has known polarization). This polarimetry method is typically reliable to about 5% relative.

Similarly, the tensor polarization is given by:

$$P_{zz} = \frac{4 + \tanh^2 \frac{\mu B}{2kT}}{3 + \tanh^2 \frac{\mu B}{2kT}} \tag{33}$$

From Eqs. 32 and 33, we find:

$$P_{zz} = 2 - \sqrt{4 - 3P_z^2}$$

29

In addition to the TE method, polarizations can be determined by analyzing NMR lineshapes as described in [28] with a typical 7% relative uncertainty. At high polarizations, the intensities of the two transitions differ, and the NMR signal shows an asymmetry R in the value of the two peaks, as shown in Fig. 11. The vector polarization is then given by:

$$P_z = \frac{R^2 - 1}{R^2 + R + 1} \tag{34}$$

and the tensor polarization is given by:

$$P_{zz} = \frac{R^2 - 2R + 1}{R^2 + R + 1} \tag{35}$$

The DNP technique produces deuteron vector polarizations of up to 60% in ND_3 and 64% in LiD [29], which corresponds to tensor polarizations of approximately 30%. The target polarization decays while in beam, so that the average polarization is less than this.

2.2.2 Depolarizing the Target

To move from polarized to unpolarized measurements, the target polarization will be annihilated using destructive NMR loop field changes and destructive DNP microwave pumping. It is also possible to remove LHe in the nose of the target to remove the polarization by heating. During unpolarized data taking the incident electron beam heating is enough to remove the thermal equilibrium polarization.

NMR measurements will be used to confirm destruction of the polarization. The target material will be held at a constant temperature, and the target field will be held at a constant magnitude for both polarized and unpolarized data collection. in order to minimize the systematic differences in the two states. To minimize systematic effects over time, the polarization condition will be switched twice in a 24 hour period.

2.2.3 The Dilution Factor

To derive the expression for the dilution factor, we first start with the ratio of polarized to unpolarized counts. In each case, the number of counts that are actually measured, neglecting the small contributions of the thin aluminium cup window materials, NMR coils, etc., are

$$N_1 = Q_1 \varepsilon_1 \mathcal{A}_1 l_1 [(\sigma_N + 3\sigma_1)p_f + \sigma_{He}(1 - p_f)], \tag{36}$$

and

$$N = Q\varepsilon\mathcal{A}l[(\sigma_N + 3\sigma)p_f + \sigma_{He}(1 - p_f)]. \tag{37}$$

where Q represents accumulated charge, ε is the dectector efficiency, $\mathcal{A}$ the cup acceptance, and l the cup length.

For this calculation we assume similar charge accumulation such that $Q \simeq Q_1$, and that the efficiencies stay constant, in which case all factors drop out of the ratio leading to

$$
\begin{aligned}
\frac{N_1}{N} &= \frac{(\sigma_N + 3\sigma_1)p_f + \sigma_{He}(1 - p_f)}{(\sigma_N + 3\sigma)p_f + \sigma_{He}(1 - p_f)} \\
&= \frac{(\sigma_N + 3\sigma(1 + A_{zz}P_{zz}/2))p_f + \sigma_{He}(1 - p_f)}{(\sigma_N + 3\sigma)p_f + \sigma_{He}(1 - p_f)} \\
&= \frac{[(\sigma_N + 3\sigma)p_f + \sigma_{He}(1 - p_f)] + 3\sigma p_f A_{zz}P_{zz}/2}{(\sigma_N + 3\sigma)p_f + \sigma_{He}(1 - p_f)} \\
&= 1 + \frac{3\sigma p_f A_{zz}P_{zz}/2}{(\sigma_N + 3\sigma)p_f + \sigma_{He}(1 - p_f)} \\
&= 1 + \frac{1}{2}f A_{zz}P_{zz},
\end{aligned}
\tag{38}
$$

where $\sigma_1 = \sigma(1 + A_{zz}P_{zz}/2)$ has ben substituted, per Eq. 16, with $P_B = 0$. It can be seen that the above result corresponds to Eq. 19.

2.2.4 Prospects for Improving the Tensor Polarization

We've assumed a tensor polarization of 20% in this proposal. This enables a significant measurement of $b_1(x)$, as shown in Fig. 7. Any improvement to the expected polarization, although not strictly necessary, would allow the addition of kinematic points, and/or improved statistical accuracy.

With this in mind, we note that it has been demonstrated that the tensor polarization can be significantly enhanced by disturbing the thermal equilibrium of the sample using a frequency modulated RF source to stimulate transitions from the m=0 level. This changes the population of the m=0 level, thus changing the tensor asymmetry. This method of 'burning holes' in the NMR line with a saturating RF field was demonstrated by deBoer [31], and Meyer [27, 3] in 1985. Bueltmann *et al.* [30] also briefly investigated this technique in 1999. This last group (Crabb-UVa) demonstrated tensor polarizations P_{zz} of about 30%, as shown in Fig. 13. However, the results were not published, and this line of research was not pursued further since there was no physics motivation for tensor polarized targets at the time. Hole burning can be performed with a coil placed around the target sample driven by an additional function generator. The coil must be oriented transversely to the main field, and should produce an RF field with an amplitude of about 2 $H_1 = 10^{-4}$ T with good uniformity [32, 33]. There must not be significant heating of the target material, and the Q-value should be below the maser threshold to avoid destructive losses.

A second method exists to simultaneously stimulate transitions from two of the deuteron's three sublevels by using two independent microwave sources tuned to the closely spaced ESR transitions. Initial unpublished studies [30] demonstrated the feasibility of this technique, with the curious caveat that the CPI microwave cavities typically used in this process have a tendency to couple and lock to a common frequency when operated in close proximity. Discussions with the manufacturer [34] have revealed that this is a well known feature of the cavities, and can be easily suppressed with isolating circuitry.
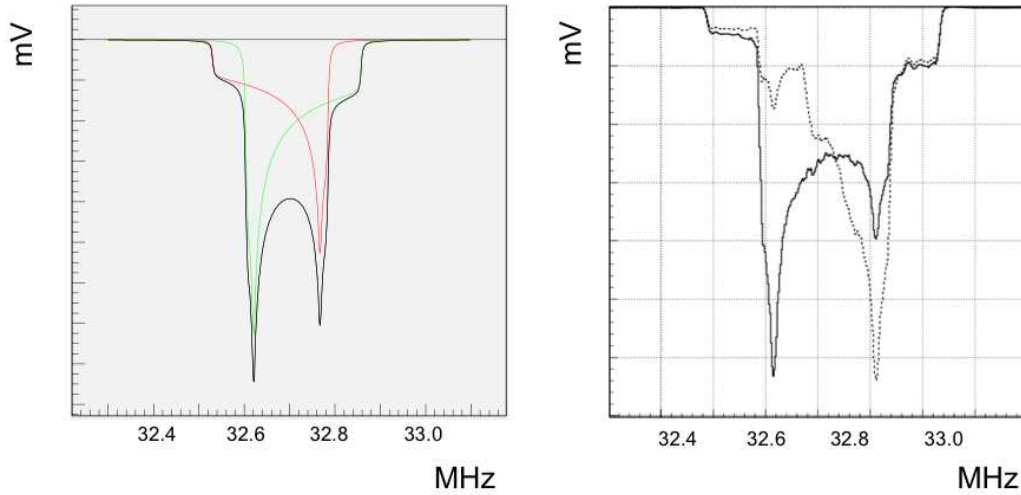
Figure 13: **Left**: Model prediction [28] of the NMR response for an ND$_3$ sample. The two discrete transitions (red and green) blend into the characteristic double peaked structure. **Right** : Demonstration of RF hole burning in ND$_3$. Solid line: ND$_3$ sample with about 30% vector polarization. Dashed line: the same sample after application of a saturating RF field, which raised the tensor polarization to $P_{zz} \approx 30\%$. Notice the strong suppression of the left peak. Reproduced from [30].

In light of these past successes, we are cautiously optimistic that atleast one of these methods will be capable of producing tensor polarizations of 30% and higher. But this will require dedicated R&D. There are several groups within our collaboration that are willing to pursue this work, but progress is unlikely to be made until there is a demonstrated physics motivation to drive the need for target development.

3 Summary

We request 30 days of production beam in order to measure the tensor asymmetry A$_{zz}$ and the spin structure function b_1 using a tensor polarized (P$_{zz}$=20%) deuteron target together with the Hall C HMS and SHMS spectrometers. All existing theoretical predictions for b_1 in the region of interest predict small or vanishing values for b_1 in contrast to the apparent large negative result of the only existing measurement from HERMES.

This experiment will provide access to the tensor quark polarization and allow a test of the Close-Kumano sum rule, which vanishes in the absence of tensor polarization in the quark sea. Until now, tensor structure has been largely unexplored, so the study of these quantities holds the potential of initiating a new field of spin physics at Jefferson Lab.

References

[1] H. Khan and P. Hoodbhoy, Phys. Rev. **C44**, 1219 (1991).

[2] S. K. Taneja, K. Kathuria, S. Liuti, and G. R. Goldstein, Phys.Rev. **D86**, 036008 (2012).

[3] W. Meyer *et al.*, Nucl. Instrum. Meth. **A244**, 574 (1986).

[4] J. Carlson and R. Schiavilla, Rev. Mod. Phys. **70**, 743 (1998).

[5] J. L. Forest *et al.*, Phys. Rev. **C54**, 646 (1996).

[6] A. Pais, Phys. Rev. Lett. **19**, 544 (1967).

[7] L. L. Frankfurt and M. I. Strikman, Nucl. Phys. **A405**, 557 (1983).

[8] P. Hoodbhoy, R. L. Jaffe, and A. Manohar, Nucl. Phys. **B312**, 571 (1989).

[9] C. Riedl, Ph. D thesis, DESY-THESIS-2005-027 (2005).

[10] A. Airapetian *et al.*, Phys. Rev. Lett. **95**, 242001 (2005).

[11] J. Edelmann, G. Piller, and W. Weise, Phys. Rev. **C57**, 3392 (1998).

[12] K. Bora and R. L. Jaffe, Phys. Rev. **D57**, 6906 (1998).

[13] S. Kumano, Phys. Rev. **D82**, 017501 (2010).

[14] G. A. Miller, In Stanford 1989, Proceedings, Electronuclear physics with internal targets 30-33 .

[15] G. A. Miller, private communication, to be published.

[16] P. J. Sutton, A. D. Martin, R. G. Roberts, and W. J. Stirling, Phys. Rev. **D45**, 2349 (1992).

[17] A. Y. Umnikov, Phys. Lett. **B391**, 177 (1997).

[18] M. Sargsian, private communication, to be published.

[19] L. L. Frankfurt and M. I. Strikman, Phys. Rept. **76**, 215 (1981).

[20] M. M. Sargsian, S. Simula, and M. I. Strikman, Phys. Rev. **C66**, 024001 (2002).

[21] F. E. Close and S. Kumano, Phys. Rev. **D42**, 2377 (1990).

[22] A. V. Efremov and O. V. Teryaev, Sov. J. Nucl. Phys. **36**, 557 (1982).

[23] S. J. Brodsky, AIP Conf.Proc. **792**, 279 (2005).

[24] S. J. Brodsky, C.-R. Ji, and G. P. Lepage, Phys.Rev.Lett. **51**, 83 (1983).

[25] D. Keller, "Uncertainty in DNP Target Data for E08-007", JLab-TN-051.

[26] C. Keith, JLab polarized target group. Private communication.

[27] W. Meyer and E. Schilling, BONN-HE-85-06, C84-09-03.1 (1985).

[28] C. Dulya *et al.*, Nucl. Instrum. Meth. **A398**, 109 (1997).

[29] S. L. Bueltmann *et al.*, Nucl. Instrum. Meth. **A425**, 23 (1999).

[30] S. Bueltmann, D. Crabb, Y. Prok. *UVa Target Studies*, UVa Polarized Target Lab technical note, 1999.

[31] W. de Boer, Cern Report CERN-74-11 (1974).

[32] P. Hautle, PhD. Thesis.

[33] P. Hautle *et al.*, Nucl.Instrum.Meth. **A356**, 108 (1995).

[34] H. Bishop, Communications and Power Industries (CPI). Personal communication.